Facile synthesis of a high purity α-MnO_2 nanorod for rapid degradation of Rhodamine B

Shumin Wang[a,*], Ao Guan[a], Jiahan Wang[a], Xiaofang Fu[a], Xiang Guo[a], Yuan Tian[b], Kaixuan Wang[b], Wenping Cao[b]

[a]*College of Light Industry, Liaoning University, Shenyang 110036, China.*

[b]*College of Chemistry, Liaoning University, Shenyang 110036, China.*

Abstract

Manganese dioxide (α-MnO_2) nanorods with diameters of about 5-15 nm and lengths of 100-150 nm were synthesized by a simple co-precipitation method. XRD, TEM, HRTEM, SAED and XPS were used to analyze the crystallographic information, microstructure and chemical bonding of the as-prepared sample. The α-MnO_2 nanorod exhibited a high efficiency and rapid removal rate of rhodamine B (RhB), which reached about 97.5% within 10 min when pH=4 (and pH=6.6) and 97.7% within 50 min when pH = 9 in the presence of H_2O_2. The results also indicated that a lower pH value is conducive to the movement of the characteristic peak and the attenuation of the intensity of the characteristic peak of RhB dye. Then a possible catalytic mechanism was revealed. Moreover, the α-MnO_2 nanorod exhibits an excellent recyclability and catalytic stability. This research indicates that α-MnO_2 nanorods have a potential application in practical dye pollutant treatment.

Keywords: α-MnO_2 nanorod, catalyst, degradation, rhodamine B

*Corresponding author:

College of Light Industry, Liaoning University, Shenyang 110036, P.R. China.

E-mail address: wangshumin@lnu.edu.cn (Shumin Wang)

1. Introduction

Random discharge of dye wastewater from the textile industries will cause toxicological and aesthetic problems, reduce the photosynthetic activity of aquatic plants, and bring about adverse effects on aquatic organisms, human health and the environment due to high chemical oxygen demand, high intensity of color, hard to degrade, high toxicity and even potential carcinogenic risk [1-5]. Rhodamine B (RhB) is a water-soluble xanthene organic dye, which contains four N-ethyl groups at either side of the xanthene ring, and it is widely used in textile, printing, photography and other industries. However, its harm to human and animals cannot be ignored, such as carcinogenicity, reproductive and developmental toxicity, chronic toxicity and so on. Therefore, it is of great concern to decompose RhB into non-toxic and pollution-free substances.

Recently, much effort has been focused on the degradation of dyes by semiconductor photocatalyst. In pursuit of low cost, non-toxicity and chemical stability, titanium dioxide (TiO_2) shows good application as a photocatalyst [6,7]. However, TiO_2 can only absorb ultraviolet (UV) light in the solar spectrum, which greatly limits the application of TiO_2 in photocatalytic degradation. Meanwhile, the dye with high concentration tends to show a dense color, which will reduce the photocatalytic efficiency due to poor light transmittance. Therefore, it is urgent to find a more effective method to achieve the degradation of organic dyes. Some reports have demonstrated that MnO_2 is expected to degrade organic dyes in different surroundings because of its superior catalytic activities and adsorption capabilities [8-17]. And the polymorphic structure of MnO_2 materials determines their catalytic performance [10-12, 18-21]. The α-MnO_2 possesses higher oxidative property than β-MnO_2 and γ-MnO_2 due to the more exposure of [MnO_6] edges in α-MnO_2. For instance, Saputra et al. have synthesized different crystallographic phases of MnO_2 materials by hydrothermal method, and they

reported that α-MnO_2 presented the highest activity in activation of Oxone® for phenol degradation than γ-MnO_2 and β-MnO_2 due to the high surface area, oxygen loss and double tunneled structure [19]. Meng et al. have reported that α-MnO_2 has higher catalytic activity in oxygen evolution reaction than β-, δ-MnO_2 and amorphous Mn oxide because of its abundant di-μ-oxo bridges, low charge transfer resistance, and strongest O_2 adsorption ability [20].

Herein, uniform-sized α-MnO_2 nanorods were synthesized by a simple method using potassium permanganate ($KMnO_4$) and manganese chloride tetrahydrate ($MnCl_2 \cdot 4H_2O$) as manganese source. In order to reveal the catalytic mechanism of α-MnO_2 on RhB dye, the efficient oxidative degradation and adsorption ability of the α-MnO_2 nanorods toward RhB at different H_2O_2 dosage (1–14 ml) and pH values (pH = 4–12) was investigated. The obtained α-MnO_2 nanorods present excellent performance in degradation of complex organic dyes.

2. Experimental

2.1. Synthesis of α-MnO_2 nanorod

All the reagents were analytical grade and used without any further purification. The α-MnO_2 nanorods were prepared by co-precipitation method with refluxing process as follows: 180 mg of $MnCl_2 \cdot 4H_2O$ was dissolved in 50 mL isopropanol under magnetic stirring at 85 ℃ and the reflux reaction was carried out simultaneously. Then $KMnO_4$ solution (127 mM, 5 mL) was added dropwise into the above-mentioned solution at a uniform rate within 5 min at 25 ℃. The mixed solution was stirred constantly at 85 ℃ for 90 min with refluxing. The as-obtained dark brown precipitates were washed with deionized water and ethanol for several times. Finally, the powder of α-MnO_2 nanorods was collected after drying in an oven at 60 ℃.

2.2. Characterization

The crystallographic information, morphology, microstructure and chemical bonding of as-prepared product were analyzed by X-ray diffraction (XRD) (Bragg-Brentano diffractometer (D8 tools) with a Cu Kα line at 0.15418 nm as a source), transmission electron microscope (TEM), high resolution transmission electron microscopy (HRTEM), selective area electron diffraction (SAED) (JEOL JEM-2100F operated at 200 kV) and X-ray photoelectron spectroscopy (XPS) (ESCALAB-250 performed with a monochromatic Al Kα (1486.6 eV) radiation source). The absorption spectrum and absorbance of different solutions were measured with a Shimadzu UV-2550 ultraviolet-visible (UV–Vis) spectrophotometer. The zero point of charge (pH_{PZC}) of the sample was analyzed by Zetasizer Nano analyzer (Malvern, UK).

2.3. Degradation of RhB

HCl or KOH solutions were used to adjust the pH values of initial RhB solutions (20 mg L^{-1}) and the degradation process of RhB was as followed: 10 mg of as-prepared α-MnO_2 nanorods was dispersed in RhB solution (50 mL) at 25 ℃. Before H_2O_2 addition, the suspension was stirred uniformly for 30 min to achieve absorption/desorption equilibrium. Then, 5 mL of the mixture solution was pipetted, centrifuged and named as 0 min. Subsequently, a certain amount of 30 % H_2O_2 was added to above suspension. At certain intervals, 5 mL of the suspension was taken out and centrifuged to remove solid nanoparticles. The clear upper layer solution was analyzed by a UV–Vis spectrophotometer.

3. Results and Discussion

3.1. The microstructure and morphology of sample

XRD was used to characterize the crystal structure and phase composition of the product, and the

corresponding results are presented in Fig. 1. The diffraction peaks at 2θ =12.6 °, 18.0 °, 25.5 °, 28.6 °, 37.4 °, 41.7 °, 49.7 °, 55.9 °, 59.8 °, 65.4 ° and 68.8 °, corresponding to the lattice spacing (d) values of approximately 0.692, 0.490, 0.346, 0.309, 0.240, 0.215, 0.183, 0.163, 0.153, 0.143 and 0.137 nm, can be characterized as the (110), (200), (220), (310), (211), (301), (411), (600), (521), (002) and (202) planes of α-MnO_2 (JCPDS-ICDD Card No. 44-0141), respectively. No peaks of any other MnO_2 phase were detected, which indicated the high purity and crystallinity of the final product.

TEM, HRTEM and SAED analyses were carried out to acquire a deeper understanding of the structural information of the as-prepared α-MnO_2. Fig. 2a displays the TEM image of α-MnO_2, revealing the nanorod-like morphology feature. It can be seen that the products were uniform nanorods with diameters of about 5-15 nm and lengths of 100-150 nm. As can be seen from the HRTEM images (Fig. 2b-d), the measured lattice distances are about 0.49, 0.24 and 0.31 nm, which correspond to the (220), (211) and (310) planes of α-MnO_2, respectively. Fig. 2e exhibits multiple diffraction rings, indicating the crystallinity of α-MnO_2 nanorods. The diffraction rings are explicitly clear for the (200), (310), (211), (301), (411), (521) and (002) planes of α-MnO_2, which agree well with the XRD results.

XPS is an excellent technique to understand the relative composition of the synthesized material and the oxidation state of the transition metal ion. The wide-scan XPS spectrum, Mn 2p, Mn 3s and O 1s spectra of as-prepared α-MnO_2 are presented in Fig. 3a-d. The peaks of $Mn2p_{1/2}$ (653.6 eV) and $Mn2p_{3/2}$ (641.8 eV) have a spin energy separation of about 11.8 eV, which reveals the presence of Mn^{4+} ions in the α-MnO_2 [9, 22-24]. The Mn 3s spectrum of as-synthesized α-MnO_2 with a peak separation of about 4.7 eV was observed, which indicates that the Mn in the sample has an oxidation state of 4 [13, 25]. In the case of oxygen (Fig. 3d), three different peaks centered at 529.3, 531.2 and 532.6 eV, which correspond to the lattice oxygen (in the form of O^{2-}), the surface adsorbed oxygen (such as OH) and H-O-H bond for residual water, respectively [24,25].

3.2. Degradation of RhB

Fig. 4a shows the UV–vis absorption spectra of RhB aqueous solution. It can be seen that only a small amount of RhB was physically adsorbed by α-MnO_2 nanorods at t=0. However, the intensity of RhB absorption peak was quickly decreased after the addition of 6 mL H_2O_2, which confirms that H_2O_2 has a certain degradation effect on RhB. The absorption peak of RhB dye at λ=553 nm (λ_{max}) shifted to 546 nm after 10 min, attributing to the formation of N-deethylated intermediates of RhB [3, 26]. And the λ_{max} completely disappeared after about 20 min, and no new absorption bands appeared in either the visible or the ultraviolet. The decolorization of RhB solution and reduction of absorption peak intensity of the intermediate product indicated that the structure of conjugated xanthene (the chromophore) has been destroyed. Fig. 4b shows the degradation efficiency of RhB in different solution systems. The concentration of RhB solution was almost the same with the extension of the reaction time when α-MnO_2 was added individually to the RhB solution, except that less than 10% of RhB was physically adsorbed by α-MnO_2 at the beginning. When 6 mL H_2O_2 was firstly added individually to the RhB solution, the degradation rate of RhB solution was 27%, and there was no further change with increasing reaction time, which confirms that H_2O_2 has a degradation effect on RhB only at the initial stage. Once the as-prepared α-MnO_2 nanorods and H_2O_2 were mixed together, significant degradation of RhB took place. About 97.5% of RhB was degraded within 10 min, which means that α-MnO_2 nanorods and H_2O_2 have synergistic effect on the catalytic degradation of RhB. At the beginning, RhB molecules and H_2O_2 are adsorbed on the surface of the α-MnO_2 nanorods [5, 8, 27-29]. And H_2O_2 was decomposed into $O_2^{\bullet-}$, $OH^{\bullet}$ or $HOO^{\bullet}$ radical species induced by the α-MnO_2 nanorods. Then the adsorbed RhB dye molecules are decomposed into small molecules by the nascent free radical species ($O_2^{\bullet-}$, $OH^{\bullet}$) with high oxidation ability. Finally, the small molecules are separated from the surface of

α-MnO_2 nanorods and the catalyst is recovered. Under the same experimental conditions, when the concentration of RhB was increased to 40 mg L^{-1}, the degradation rate of RhB was 94.4% after 80 min, which indicated that the α-MnO_2 nanorods had good degradation effect on RhB solution with higher concentration. However, compared with RhB with 20 mg L^{-1}, the degradation rate was lower because of insufficient free radical species in the reaction system.

Fig. 5a shows the degradation efficiency of RhB solution (20 mg L^{-1}) with different H_2O_2 dosage. It can be seen that when 1 mL H_2O_2 is added, the degradation rate of RhB reaches 60% in a short time of 5 min, and a large number of pink bubbles are observed in the solution, which indicates that the reaction is violent. After that, the degradation rate remained unchanged, indicating that the content of H_2O_2 in the solution system was insufficient, and the radical species reaction was completed. When the amount of H_2O_2 increased from 1 mL to 14 mL, the degradation rate of the RhB solution increased from 60% to nearly 100% after 5 min. Comparing the degradation rates of all reaction systems within 20 min, we found that the degradation rate was 91.8%, 97.4% and 98.8% when the H_2O_2 dosage was 2 , 4 and 6 mL, respectively, which indicated that the increase of H_2O_2 dosage in a certain range would increase the content of $O_2^{\bullet-}$ and $OH^{\bullet}$ radical species in the system, and then make more RhB degraded, that is, the degradation rate of RhB increased. When the amount of H_2O_2 is 8 mL and 14 mL, the degradation rate is faster, but the color change of the whole reaction system is not as good as that of the 6 mL and the color of the 6 mL group shows a ladder shape from deep to shallow, which is easy to observe.

The stability and reusability of catalyst is indispensable for its practical application. Therefore, the recycling reactions of the α-MnO_2 nanorods in degradation of RhB were carried out (Fig. 5b). The α-MnO_2 nanorods exhibited almost the same catalytic activity with the increase of recycling times,

which indicated that the obtained α-MnO_2 nanorods possess high stability in RhB degradation. In order to grasp the changes of α-MnO_2 nanorods after catalytic reaction, the XRD and TEM were used to analyze the recycled α-MnO_2 catalyst. As shown in Fig. 6a-b, there is no significant difference between the reacted and fresh sample, suggesting that α-MnO_2 nanorods have high stability and potential application prospect in degradation of organic dyes.

As shown in Fig. 7, pH value plays a very important role in the degradation of RhB solution. The characteristic peak (λ_{max} =553 nm) of RhB decreased significantly as well as a blue shift from 553 to 544 nm after 10 min when pH=4 (Fig. 7a), similar with the case of pH=6.6 (Fig. 4a). For pH=9 and pH=12, there is nearly no shifted of characteristic peak with increasing interaction time (Fig. 7b and 7c), suggesting no generation of N-deethylated intermediates of RhB. It is well known that the surface charge of catalyst depends largely on the pH value of the solution [1,30-32]. The pH_{PZC} of α-MnO_2 nanorods is determined to be 3.08 (Fig. 7e), above which the surface charge was negative because of the deprotonation reaction, and this would facilitate the adsorption of cationic RhB on α-MnO_2 nanorods. In addition, elevating solution pH would increase the amount of surface negative charges. Therefore, the removal of RhB dye could be attributed to the oxidative degradation and adsorption decolorization when pH< 9. Then, the oxidative degradation was gradually weakened and adsorption decolorization played a leading role in the degradation mechanism with the increase of pH values. According to the above discussion, the possible degradation mechanism is illustrated in Fig. 8. Fig. 7d shows the removal percentage of RhB by α-MnO_2 nanorods at different pH values. The removal efficiency of RhB at pH=4 and pH=6.6 is much higher than that at pH=9 within 10 min (97.5% removed at pH=4 and pH=6.6, while 87.7% removed at pH=9), but eventually reached similar degradation efficiency within 50 min. However, the removal efficiency is just less than 80% after 150

min in the case of pH=12. Apparently, low pH value is beneficial to degrade RhB dye.

4. Conclusions

A high purity α-MnO_2 nanorod has been synthesized by a simple co-precipitation method using potassium permanganate and manganese chloride tetrahydrate as manganese source. The α-MnO_2 nanorod exhibited a high efficiency and rapid removal of RhB. Furthermore, a lower pH value is conducive to the movement of the characteristic peak and the attenuation of the intensity of the characteristic peak. The RhB removal rate reached as high as 97.5% within 10 min (pH = 4 and 6.6) and 97.7% within 50 min (pH = 9), indicating that α-MnO_2 nanorod has more extensive application for RhB removal both in acid and alkaline conditions. Subsequently, the possible decolorization mechanism was proposed. The removal of RhB is attributed to the combination of oxidation and adsorption. It is believed that α-MnO_2 nanorods synthesized by such a simple and convenient approach holds great promise for the degradation of dye wastewater in practical application.

Acknowledgments

This work was supported by the National Natural Science Foundation of China [grant number 51602140]; the Natural Science Foundation of Liaoning Province (grant number 2019-ZD-0189), the Liaoning Province Doctor Startup Fund [grant number 201601093]; the Scientific Research Fund of Liaoning Provincial Education Department [grant number LYB201619].

References

[1] A. Gagrani, J.W. Zhou, T. Tsuzuki, Solvent free mechanochemical synthesis of MnO_2 for the

efficient degradation of Rhodamine B. Ceram. Int. **44**, 4694–4698 (2018)

[2] G.X. Zhao, J.X. Li, X.M. Ren, J. Hu, W.P. Hu, X.K. Wang, Highly active MnO_2 nanosheet synthesis from graphene oxide templates and their application in efficient oxidative degradation of methylene blue. RSC Adv. **3**, 12909–12914 (2013)

[3] H.Sun, K.L. Xu, M.J. Huang, Y.X. Shang, P. She, S.Y. Yin, Z.N. Liu, One-pot synthesis of ultrathin manganese dioxide nanosheets and their efficient oxidative degradation of Rhodamine B. Appl. Sur. Sci. **357**, 69–73 (2015)

[4] R.S. Dassanayake, E. Rajakaruna, H. Moussa, N. Abidi, One-pot synthesis of MnO_2–chitin hybrids for effective removal of methylene blue. Int. J. Biol. Macromol. **93**, 350–358 (2016)

[5] K. Yu, S.G. Yang, H. He, C. Sun, C.G. Gu, Y.M. Ju, Visible light-driven photocatalytic degradation of rhodamine B over $NaBiO_3$: pathways and mechanism. J. Phys. Chem. A **113**, 10024–10032 (2009)

[6] M. Thabit, H.L. Liu, J. Zhang, B. Wan, Pd-MnO_2 nanoparticles/TiO_2 nanotube arrays (NTAs) photo-electrodes photo-catalytic properties and their ability of degrading Rhodamine B under visible light. J. Environ. Sci. **60**, 53–60 (2017)

[7] S.Y. Lee, D. Kang, S. Jeong, H.T. Do, J.H. Kim, Photocatalytic Degradation of Rhodamine B Dye by TiO_2 and Gold Nanoparticles Supported on a Floating Porous Polydimethylsiloxane Sponge under Ultraviolet and Visible Light Irradiation. ACS Omega **5**, 4233-4241 (2020)

[8] C.L. Yu, G. Li, L.F. Wei, Q.Z. Fan, Q. Shu, J.C. Yu, Fabrication, characterization of β-MnO_2 microrod catalysts and their performance in rapid degradation of dyes of high concentration. Catal. Today **224**, 154-162 (2014)

[9] J.Y. Qu, L. Shi, C.X. He, F. Gao, B.B. Li, Q. Zhou, H. Hu, G.H. Shao, X.Z. Wang, J.S. Qiu, Highly effificient synthesis of graphene/MnO_2 hybrids and their application for ultrafast oxidative

decomposition of methylene blue. Carbon **66**, 485–492 (2014)

[10] M. Sun, B. Lan, T. Lin, G. Cheng, F. Ye, L. Yu, X.L. Cheng, X.Y. Zheng, Controlled synthesis of nanostructured manganese oxide: crystalline evolution and catalytic activities. CrystEngComm **15**, 7010–7018 (2013)

[11] K.Z. Li, J.J. Chen, Y. Peng, W.C. Lin, T. Yan and J.H. Li, The relationship between surface open cells of α-MnO_2 and CO oxidation ability from a surface point of view. J. Mater. Chem. A **5**, 20911–20921 (2017)

[12] B.B. He, C. Gao, S.F. Zhao, X.H. Zeng, Y.F. Li, R.N. Yang, M. Sun, L. Yu, Controlled synthesis of tunnel-structured MnO_2 through hydrothermal transformation of δ-MnO_2 and their catalytic combustion of dimethyl ether. J. Solid State Chem. **269**, 305–311 (2019)

[13] F. W. Boyom-Tatchemo, F. Devred, G. Ndiffo-Yemeli, S. Laminsi, E. M. Gaigneaux, Plasma-induced redox reactions synthesis of nanosized α-, γ- and δ-MnO_2 catalysts for dye degradation. Appl. Catal. B: Environ. **260**, 118159 (2020)

[14] S. M. Husnain, U. Asim, A. Yaqub, F. Shahzad, N. Abbas, Recent trends of MnO_2-derived adsorbents for water treatment: a review. New J. Chem. **44**, 6096–6120 (2020)

[15] S. Khalid, C.B Cao, Facile synthesis of 3D hierarchical MnO_2 microspheres and their ultrahigh removal capacity for organic pollutants. New J. Chem. **41**, 5794–5801 (2017)

[16] R. Maria-Hormigos, M. Pacheco, B. Jurado-Sánchez, A. Escarpa, Carbon nanotubes–ferrite–manganese dioxide micromotors for advanced oxidation processes in water treatment. Environ. Sci.: Nano **5**, 2993–3003 (2018)

[17] Y. G. Kang, H. Yoon, C. S. Lee, E. J. Kim, Y. S. Chang, Advanced oxidation and adsorptive bubble separation of dyes using MnO_2–coated Fe_3O_4 nanocomposite. Water Res. **151**, 413–422 (2019)

[18] J.Z. Huang, S.F. Zhong, Y.F. Dai, C.C. Liu, H.C. Zhang, Effect of MnO_2 phase structure on the oxidative reactivity toward bisphenol a degradation. Environ. Sci. Technol. **52**, 11309–11318 (2018)

[19] E. Saputra, S. Muhammad, H. Sun, H.M. Ang, M. Tade, S. Wang, Different crystallographic one-dimensional MnO_2 nanomaterials and their superior performance in catalytic phenol degradation. Environ. Sci. Technol. **47**, 5882–5887 (2013)

[20] Y.T. Meng, W.Q. Song, H. Huang, Z. Ren, S.Y. Chen, S.L. Suib, Structure-property relationship of bifunctional MnO_2 nanostructures: highly efficient, ultra-stable electrochemical water oxidation and oxygen reduction reaction catalysts identified in alkaline media. J. Am. Chem. Soc. **136**, 11452–11464 (2014)

[21] B.T. Zhang, G. Cheng, W.J. Ye, X.Y. Zheng, H.F. Liu, M. Sun, L. Yu, Y.Y. Zheng, X.L. Cheng, Rational design of MnO_2 @MnO_2 hierarchical nanomaterials and their catalytic activities. Dalton Trans. **45**, 18851–18858 (2016)

[22] V. Subramanian, H.W. Zhu, R. Vajtai, P.M. Ajayan, B.Q. Wei, Hydrothermal Synthesis and Pseudocapacitance Properties of MnO_2 Nanostructures. J. Phys. Chem. B **109**, 20207–20214 (2005)

[23] K. Mishra, T.N. Poudel, N. Basavegowda, Y.R. Lee, Enhanced catalytic performance of magnetic Fe_3O_4-MnO_2 nanocomposites for the decolorization of rhodamine B, reduction of 4-nitroaniline, and sp^3 C–H functionalization of 2-methylpyridines to isatins. J. Catal. **344**, 273–285 (2016)

[24] Y.R. Wang, X.F. Zhang, X. He, W. Zhang, X.X. Zhang, C.H. Lu, In situ synthesis of MnO_2 coated cellulose nanofibers hybrid for effective removal of methylene blue. Carbohyd. Polym. **110**, 302–308 (2014)

[25] P. Mahamallik, S. Saha, A. Pal, Tetracycline degradation in aquatic environment by highly porous MnO_2 nanosheet assembly. Chem. Eng. J. **276**, 155–165 (2015)

[26]T. Watanabe, T. Takizawa, K. Honda, Photocatalysis through excitation of adsorbates. 1. Highly efficient N-deethylation of rhodamine B adsorbed to cadmium sulfide. J. Phys. Chem. **81**, 1845–1851 (1977)

[27] J. Han, M.G. Wang, S.Y. Cao, P. Fang, S. Lu, R. Chen, R. Guo, Reactive template strategy for fabrication of MnO_2/polyaniline coaxial nanocables and their catalytic application in the oxidative decolorization of rhodamine B. J. Mater. Chem. A **1**, 13197–13202 (2013)

[28] A.L.T. Pham, F.M. Doyle, D.L. Sedlak, Inhibitory Effect of Dissolved Silica on H_2O_2 Decomposition by Iron(III) and Manganese(IV) Oxides: Implications for H_2O_2-Based In Situ Chemical Oxidation. Environ. Sci. Technol. **46**, 1055–1062 (2012)

[29] W.X. Zhang, Z.H. Yang, X. Wang, Y.C. Zhang, X.G. Wen, S.H. Yang, Large-scale synthesis of β-MnO_2 nanorods and their rapid and efficient catalytic oxidation of methylene blue dye. Catal. Commun. **7**, 408–412 (2006)

[30] Y. He, D.B. Jiang, J. Chen, D.Y. Jiang, Y.X. Zhang, Synthesis of MnO_2 nanosheets on montmorillonite for oxidative degradation and adsorption of methylene blue. J. Colloid Interf. Sci. **510**, 207–220 (2018)

[31] M.A.M. Khraisheh, M.A. Al-Ghouti, S.J. Allen, M.N.M. Ahmad, The effect of pH,temperature, and molecular size on the removal of dyes from textile effluentusing manganese oxides-modified diatomite. Water Environ. Res. **76**, 2655–2663 (2004)

[32] J. Deng, Y.J. Ge, C.Q. Tan, H.Y. Wang, Q.S. Li, S.Q. Zhou, K.J. Zhang, Degradation of ciprofloxacin using α-MnO_2 activated peroxymonosulfate process: Effect of water constituents, degradation intermediates and toxicity evaluation. Chem. Eng. J. **330**, 1390–1400 (2017)

Figure captions

Fig. 1 XRD pattern of as-prepared α-MnO_2 nanorods.

Fig. 2 TEM (a), HRTEM (b)–(d) and SAED (e) images for α-MnO_2 nanorods.

Fig. 3 XPS spectra for α-MnO_2 Nanorods. (a) Wide-scan mode, (b) Mn 2p, (c) Mn 3s and (d) O 1s.

Fig. 4 (a) UV–vis absorption spectra of RhB solution (20 mg L^{-1}) after different time intervals under 6 ml of 30 % H_2O_2 at pH=6.6, inset shows the decolorization effect of RhB solution. (b) The concentration of RhB as a function of time in different solution systems (pH=6.6).

Fig. 5 (a) The concentration of RhB as a function of time under different H_2O_2 dosage at pH=6.6. (b) Stability test of the α-MnO_2 nanorods in degradation of RhB dye. Reaction conditions: 6 mL of 30 % H_2O_2, 50 mL of RhB solution (20 mg L^{-1}), pH=6.6, reaction time of 20 min.

Fig. 6 (a) XRD pattern and (b) TEM image of α-MnO_2 nanorods after degradation reaction.

Fig. 7 (a) UV–vis absorption spectral changes of RhB solution at different pH values: (a) pH=4, (b) pH=9, (c) pH=12. (d) Time profiles of RhB removal at different pH values. Insets (a–c) are the corresponding photographs of RhB solution after decolorization. Reaction conditions: 6 mL of 30 % H_2O_2, 50 mL of RhB solution (20 mg L^{-1}). (e) The zero point of charge (pH_{PZC}) of α-MnO_2 nanorods.

Fig. 8 Schematic illustration of proposed mechanism of the α-MnO_2 nanorods in degradation of RhB.

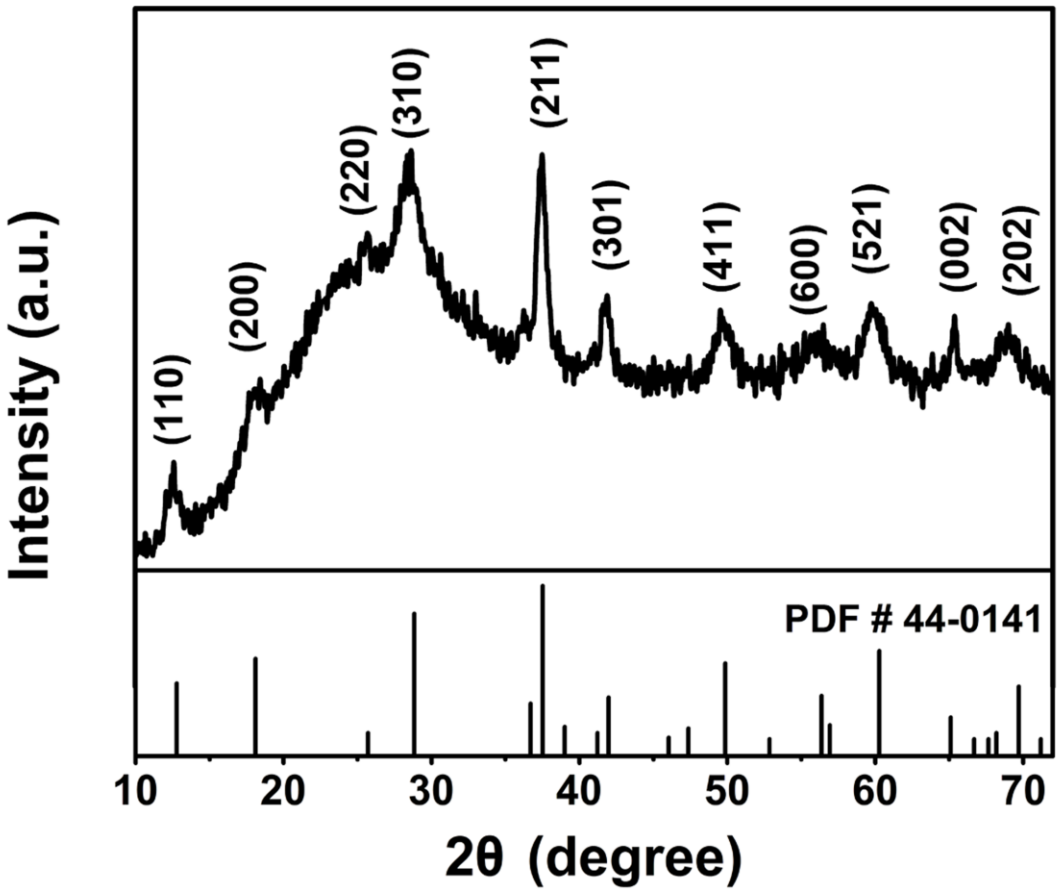
Intensity (a.u.)
(110)
(200)
(220)
(310)
(211)
(301)
(411)
(600)
(521)
(002)
(202)
PDF # 44-0141
10
20
30
40
50
60
70
2θ (degree)

Fig.1

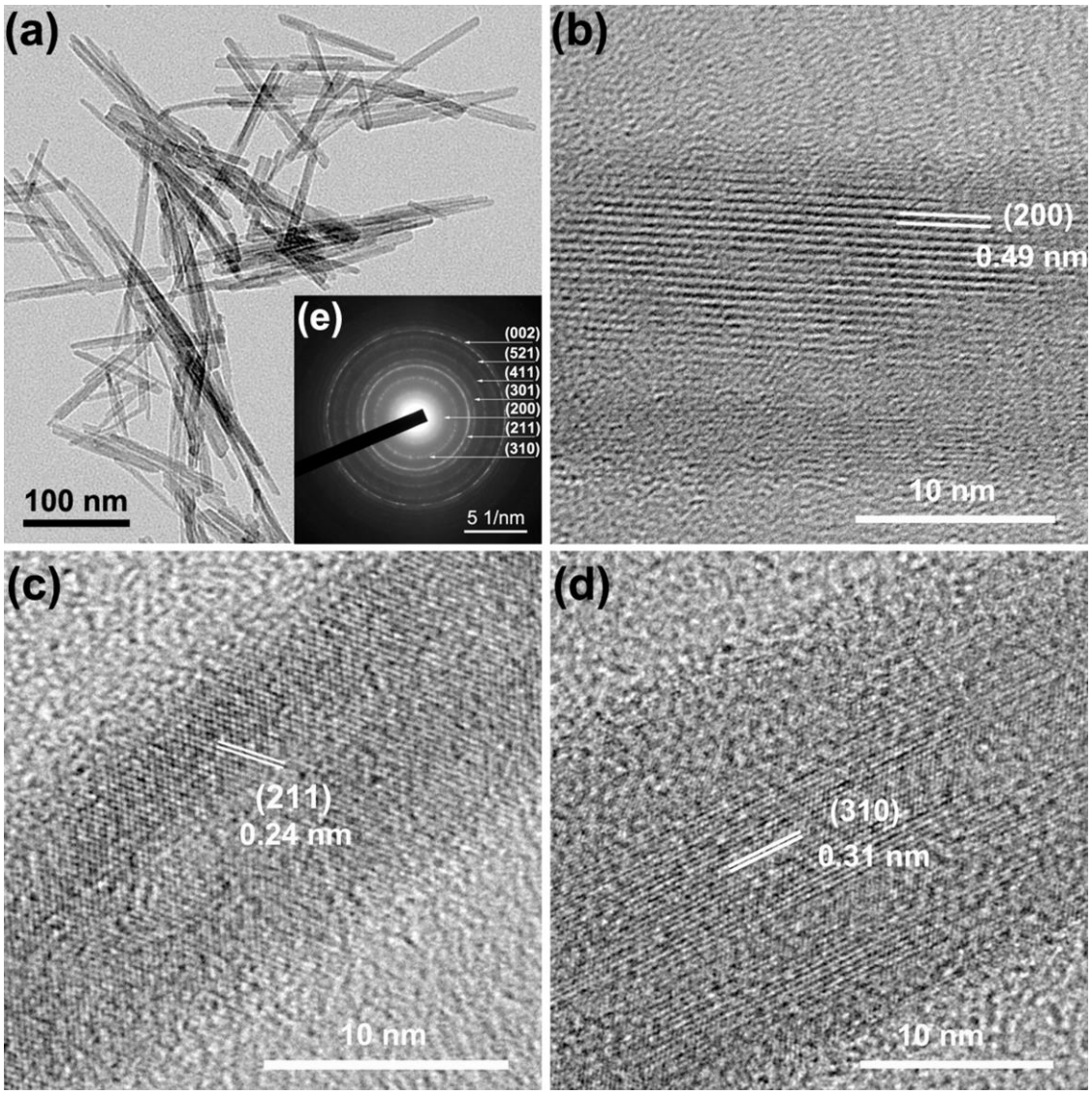
(a)
100 nm
(e)
(002)
(521)
(411)
(301)
(200)
(211)
(310)
5 1/nm
(b)
(200)
0.49 nm
10 nm
(c)
(211)
0.24 nm
10 nm
(d)
(310)
0.31 nm
10 nm

Fig.2

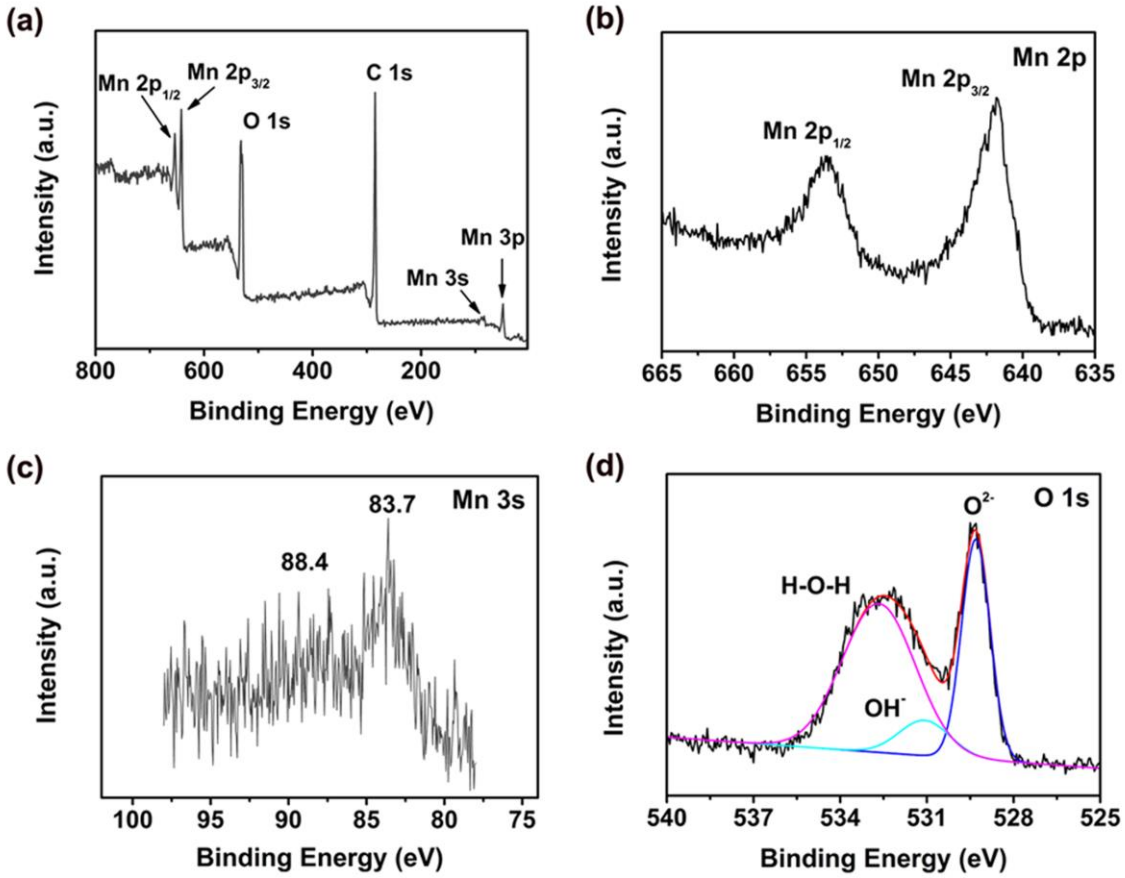
(a)
Mn 2p1/2
Mn 2p3/2
O 1s
C 1s
Mn 3p
Mn 3s
Intensity (a.u.)
800
600
400
200
Binding Energy (eV)
(b)
Mn 2p
Mn 2p3/2
Mn 2p1/2
Intensity (a.u.)
665
660
655
650
645
640
635
Binding Energy (eV)
(c)
83.7
Mn 3s
88.4
Intensity (a.u.)
100
95
90
85
80
75
Binding Energy (eV)
(d)
O2-
O 1s
H-O-H
OH-
Intensity (a.u.)
540
537
534
531
528
525
Binding Energy (eV)

Fig.3

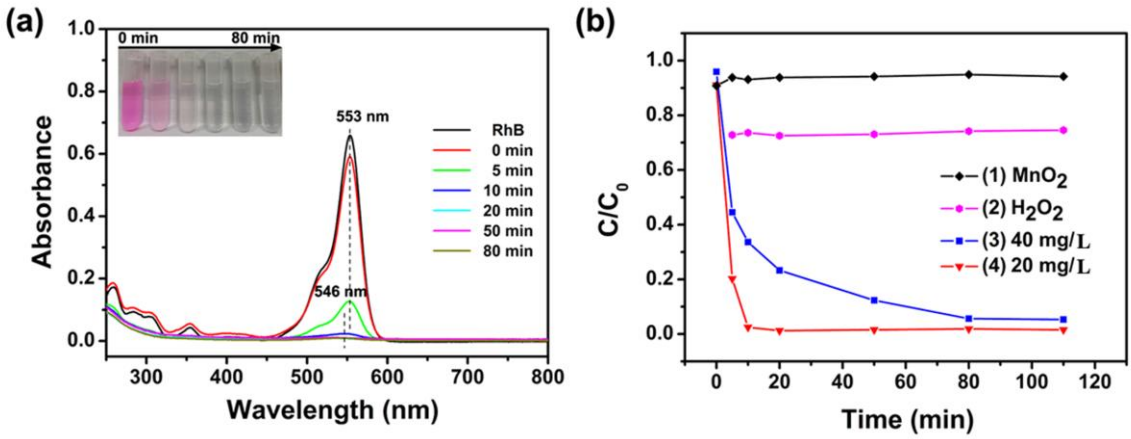
(a)
0 min
80 min
553 nm
546 nm
RhB
0 min
5 min
10 min
20 min
50 min
80 min
Absorbance
Wavelength (nm)
(b)
C/C0
(1) MnO2
(2) H2O2
(3) 40 mg/L
(4) 20 mg/L
Time (min)

Fig.4

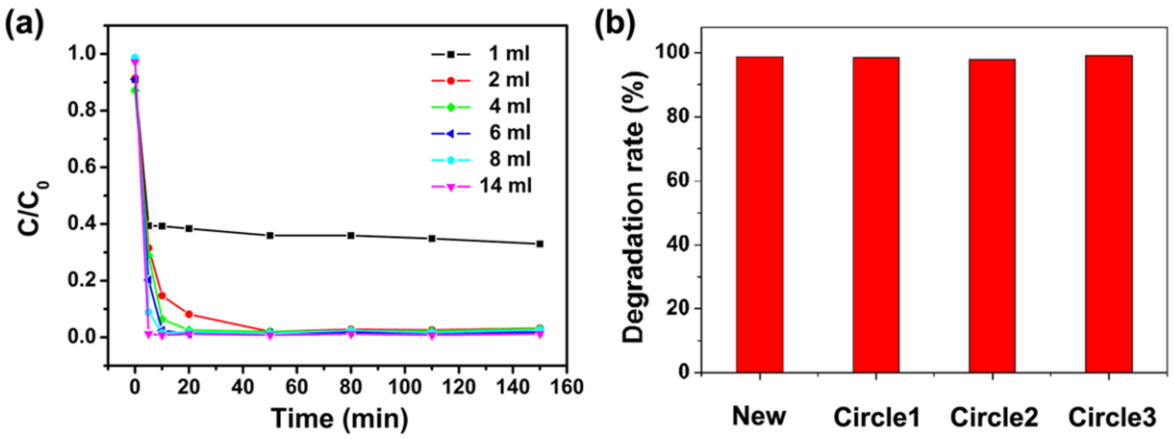
(a)
C/C0
Time (min)
1 ml
2 ml
4 ml
6 ml
8 ml
14 ml
(b)
Degradation rate (%)
New
Circle1
Circle2
Circle3

Fig.5

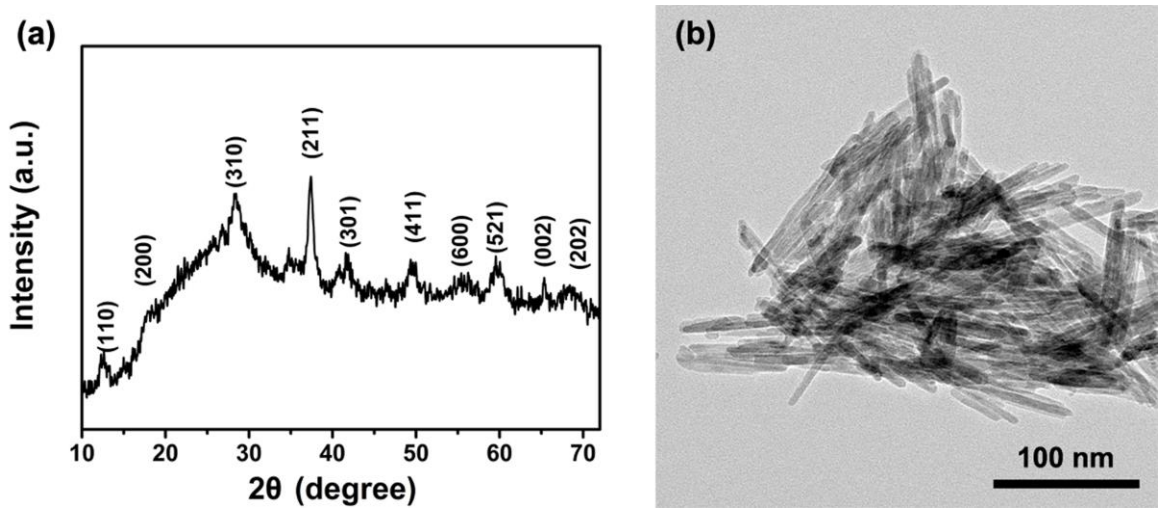
(a)
Intensity (a.u.)
(110)
(200)
(310)
(211)
(301)
(411)
(600)
(521)
(002)
(202)
10
20
30
40
50
60
70
2θ (degree)
(b)
100 nm

Fig.6

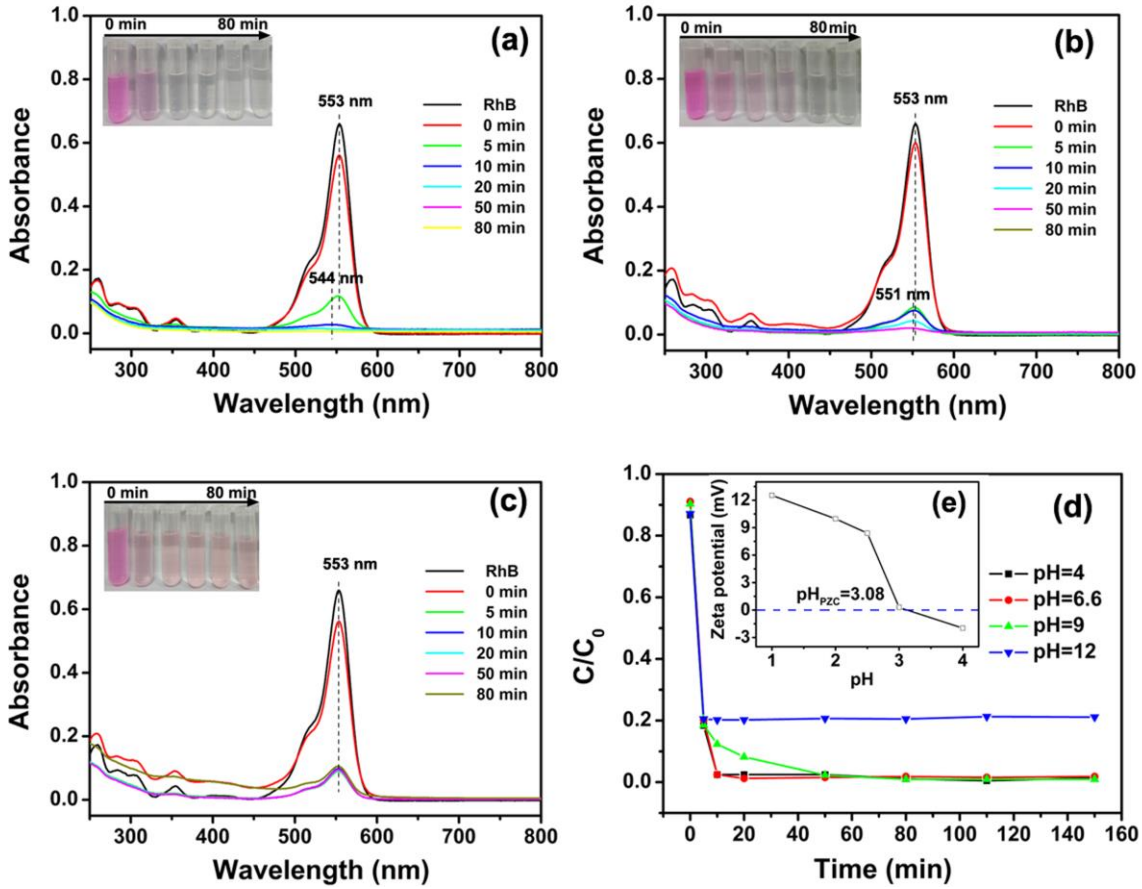
(a)
0 min
80 min
553 nm
544 nm
RhB
0 min
5 min
10 min
20 min
50 min
80 min
Absorbance
Wavelength (nm)
(b)
0 min
80 min
553 nm
551 nm
RhB
0 min
5 min
10 min
20 min
50 min
80 min
Absorbance
Wavelength (nm)
(c)
0 min
80 min
553 nm
RhB
0 min
5 min
10 min
20 min
50 min
80 min
Absorbance
Wavelength (nm)
(d)
(e)
Zeta potential (mV)
pH$_{PZC}$=3.08
pH
pH=4
pH=6.6
pH=9
pH=12
C/C$_0$
Time (min)

Fig7

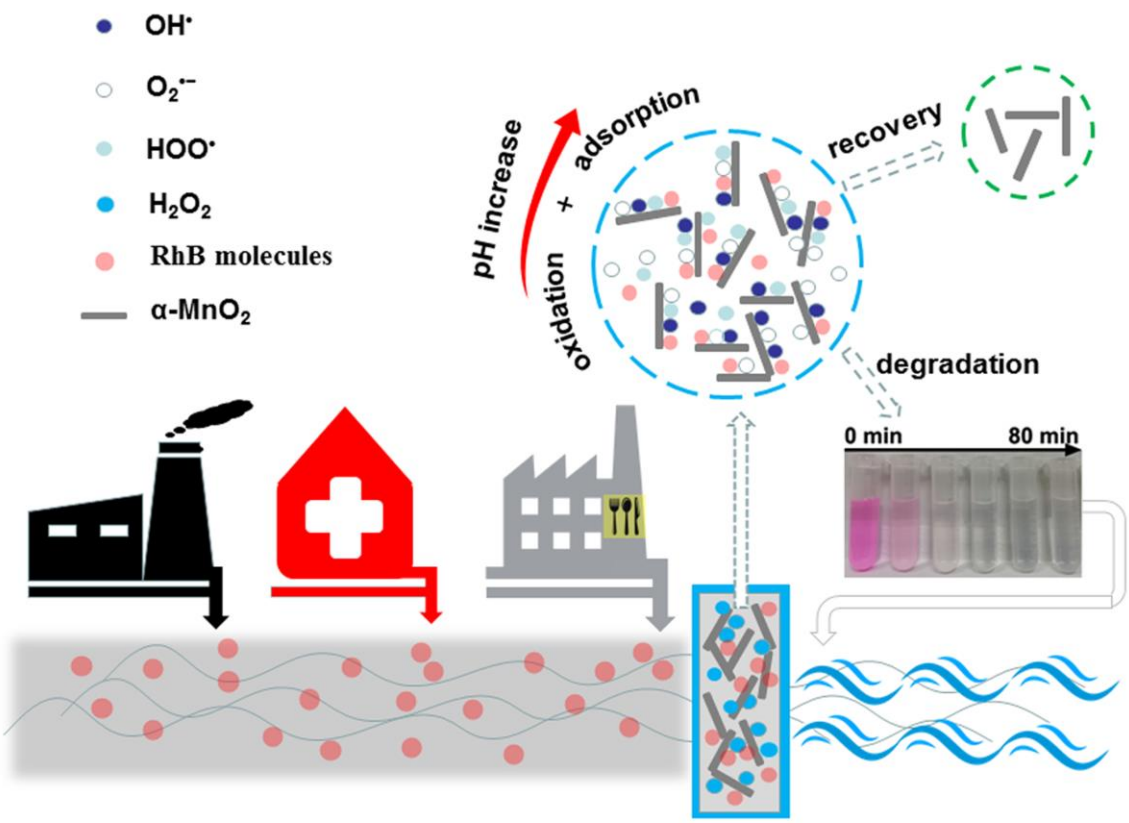
OH·
$O_2^{\cdot-}$
HOO·
H_2O_2
RhB molecules
α-MnO_2
pH increase
oxidation
+
adsorption
recovery
degradation
0 min
80 min

Fig.8